Shell-shaped Bose-Einstein condensates based on dual-species mixtures

A. Wolf [1,*] P. Boegel [2] M. Meister [1] A. Balaž [3] N. Gaaloul [4] and M. A. Efremov [1,2]

[1] *Institute of Quantum Technologies, German Aerospace Center (DLR), 89081 Ulm, Germany*

[2] *Institut für Quantenphysik and Center for Integrated Quantum Science and Technology (IQ^{ST}), Universität Ulm, 89081 Ulm, Germany*

[3] *Institute of Physics Belgrade, University of Belgrade, 11080 Belgrade, Serbia*

[4] *Institut für Quantenoptik, Leibniz Universität Hannover, 30167 Hannover, Germany*

(Received 10 November 2021; revised 8 April 2022; accepted 3 June 2022; published 11 July 2022)

Ultracold quantum gases confined in three-dimensional bubble traps are promising tools for exploring many-body effects on curved manifolds. As an alternative to the conventional technique of radio-frequency dressing, we propose to create such shell-shaped Bose-Einstein condensates in microgravity based on dual-species atomic mixtures, and we analyze their properties as well as the feasibility of realizing symmetrically filled shells. Beyond similarities with the radio-frequency dressing method, as in the collective excitation spectrum, our approach has several natural advantages like the robustness of the created quantum bubbles and the possibility of magnifying shell effects through an interaction-driven expansion.

DOI: 10.1103/PhysRevA.106.013309

I. INTRODUCTION

Motivated by the launch of NASA's Cold Atom Lab [1,2] to the International Space Station and subsequent first experiments towards shell-shaped quantum gases in microgravity [3,4], the field of many-body physics on shell topologies has recently experienced huge progress also from the theoretical side. Indeed, investigating ultracold quantum gases on a shell leads to new insights into a broad range of nontrivial quantum phenomena, such as Bose-Einstein condensation [5–9], atom lasers [10,11], superfluidity [12], vortices [13–16], and the Berezinskii-Kosterlitz-Thouless transition [17,18]. In particular, quantum gases confined to the surface of a sphere show lower condensation temperatures than their filled counterparts and the thin-shell transition between a three-dimensional and quasi-two-dimensional geometry drastically changes the collective excitations [19,20] and the dynamics of vortex-antivortex pairs [15,16].

So far, radio-frequency (rf) dressing is the primary technique being considered to experimentally realize shell-shaped Bose-Einstein condensates (BECs) in microgravity. This method, originally proposed by Zobay and Garraway [21–25], relies on the adiabatic deformation of a typically anisotropic static magnetic trap by applying an rf field and has been successful in creating a number of novel topologies and applications for BECs [26–38] on Earth. However, a three-dimensional hollow sphere of atoms is beyond the capabilities of Earth-based laboratories due to gravity pulling the atoms towards the bottom of the trap [26]. Although first results from microgravity experiments [4] promise to make shell-shaped BECs experimentally feasible, fully symmetric shells are still a very challenging task, because any inhomogeneity of the rf field and nonperfect spatial alignment with respect to the static field potentially open the shell up, similar to gravity on Earth.

Therefore, as an alternative to rf dressing, we propose to realize shell-shaped BECs employing a mixture of two atomic species. If the repulsive interspecies interaction outweighs the repulsive intraspecies one, the mixture separates into two domains, each containing solely one type of atoms [39,40]. Confining such a mixture in a three-dimensional harmonic trap leads to a regime where one species forms a shell around the other one [41–43]. The scheme can be realized with an optical dipole trap [44] to confine the atoms and a homogeneous magnetic field to tune the atom-atom interaction via Feshbach resonances [45,46]. This realization has several advantages: (i) the atoms condense into the shell-shaped ground state instead of being adiabatically deformed into it, (ii) a homogeneous Feshbach field is much easier realized than combining multiple magnetic fields for rf dressing, (iii) spherical symmetry of the atom cloud can be straightforwardly achieved by combining three optical trapping beams, (iv) an implementation on Earth is in principle feasible by optically compensating the gravitational sag, and (v) expanding shells are created by simply turning off the common trap because an inwards expansion of the outer species is prevented by the core one.

In this article we show that the mixture-based scheme is a viable alternative by finding both similarities with key properties of rf-dressed shells and a promising robustness against shell opening due to gravity. We identify the parameters required to realize shell-shaped ground states and investigate the collective excitation spectrum to give evidence that there is indeed a transition from a filled sphere to a shell-shaped BEC. The free expansion dynamics is also studied here to highlight an important difference between the two approaches, namely the presence of an inner core, which enables one to choose between two distinct scenarios depending on the interspecies interaction.

*Corresponding author: a.wolf@dlr.de

In Sec. II we present our scheme in detail and quantify conditions for the realization of an ideal spherically symmetric shell-shaped BEC based on a dual-species mixture. Section III addresses the behavior of the collective excitation frequencies as a function of the interspecies interaction. In Sec. IV, we explore two free expansion scenarios which arise due to changing the interspecies interaction. Here we find a novel regime where the shell structure is conserved during dynamics, offering in principle a way to create a shell of any desirable radius. Section V deals with the robustness of our scheme against shell-opening induced by a residual gravitational acceleration. Several already existing experimental platforms are compared and the influence of the trap frequency and atom number on the robustness is investigated. We conclude in Sec. VI by summarizing our results and discussing potential applications of our scheme in related research areas. To keep our article self-contained, but focused on the central ideas, we consider the Bogoliubov–de Gennes equations and provide description of the numerical simulations in Appendix A. Moreover, in Appendix B we compare the mixture-based scheme with the rf-dressed one, by extending our study of the ground state, collective excitation spectrum, free expansion, and feasibility.

II. SHELL-SHAPED GROUND STATES

For a BEC well below the critical temperature, its properties can be described by a mean-field approach, leading to the Gross-Pitaevskii equation (GPE) [12,47] for the condensate wave function ψ. In the case of BECs containing multiple components $\alpha = 1, 2, \ldots$ (e.g., different atomic species), the GPE for component α reads [39]

$$i\hbar\frac{\partial\psi_\alpha(\mathbf{x},t)}{\partial t} = \left[h_\alpha(\mathbf{x}) + \sum_\beta g_{\alpha\beta}|\psi_\beta(\mathbf{x},t)|^2\right]\psi_\alpha(\mathbf{x},t). \quad (1)$$

Here $h_\alpha(\mathbf{x}) = -\hbar^2\nabla^2_{\mathbf{x}}/(2m_\alpha) + V_\alpha(\mathbf{x})$ is the single-particle Hamiltonian of an atom with mass m_α and $V_\alpha(\mathbf{x})$ is the component-dependent external potential. The sum over all components in Eq. (1) contains the self-interaction of the component ($\beta = \alpha$) and the interaction between two components ($\beta \neq \alpha$). The interaction parameters $g_{\alpha\beta} = 2\pi\hbar^2 a_{\alpha\beta}(m_\alpha + m_\beta)/(m_\alpha m_\beta)$ are determined by the s-wave scattering lengths $a_{\alpha\beta} = a_{\beta\alpha}$. The condensate wave function ψ_α is normalized to the number of particles $N_\alpha = \int d^3x|\psi_\alpha(\mathbf{x},t)|^2$.

To create a shell-shaped BEC, we propose to use a two-component BEC mixture in a spherically symmetric harmonic confinement $V_\alpha(\mathbf{x}) = m_\alpha\omega_{0,\alpha}^2\mathbf{x}^2/2$ with the trap frequency $\omega_{0,\alpha}$, created by an optical dipole trap [44]. Using magnetic Feshbach resonances [45,46], we require that $g_{12} \geqslant \sqrt{g_{11}g_{22}}$ with $g_{\alpha\alpha} > 0$. In this phase-separation regime the intercomponent repulsion outweighs the intracomponent repulsion. The system therefore favors a separation of the components and reduces their overlap [40]. Combined with the harmonic confinements, the ground state of the coupled GPEs (1) is given by one component forming a shell with the other one as its core [41–43].

TABLE I. Parameters of our reference case, based on an optically trapped ^{87}Rb-^{41}K BEC mixture with laser wavelength of 1064 nm and exploiting a Feshbach resonance at 78.9 G to tune the interspecies interaction. Here $a_0 = 5.29 \times 10^{-11}$ m is the Bohr radius.

Species	N_α	$\omega_{0,\alpha}$ (Hz)	$a_{\alpha\alpha}$ (units of a_0)	$a_{\mathrm{Rb,K}}$ (units of a_0)
^{41}K	10^5	$2\pi \times 70.0$	60	85
^{87}Rb	10^6	$2\pi \times 51.3$	100	

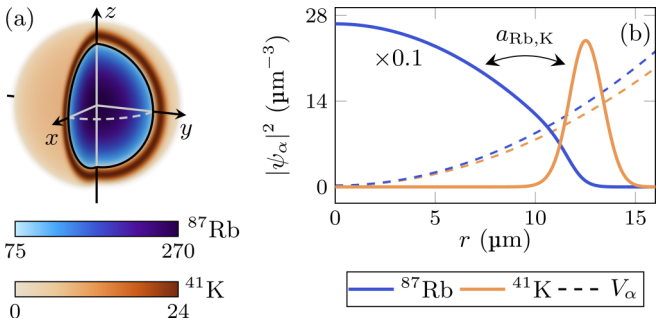

FIG. 1. Shell-shaped ground-state density distribution $|\psi_\alpha|^2$ of a spherically symmetric ^{87}Rb-^{41}K BEC mixture for the parameters presented in Table I. (a) Cut-open three-dimensional density plot (color bar units in μm^{-3}). (b) Density profiles (solid lines) along the radial direction and corresponding trapping potentials V_α (dashed lines). The interplay between the harmonic confinement and the interspecies repulsion, due to a positive s-wave scattering length $a_{\mathrm{Rb,K}}$, leads to ^{41}K (orange) forming a shell around ^{87}Rb (blue).

Here we consider the parameters listed in Table I as the reference case of our analysis. Choosing ^{87}Rb and ^{41}K is inspired by the upcoming BECCAL (Bose-Einstein Condensate and Cold Atom Lab) apparatus [48], which will provide optically trapped BEC mixtures of these species in microgravity on board the International Space Station. For ^{87}Rb-^{41}K mixtures, there is a magnetic Feshbach resonance at 78.9 G [49], around which the intercomponent scattering length $a_{\mathrm{Rb,K}}$ can be tuned to a great extent whereas the intracomponent scattering lengths $a_{\mathrm{Rb,Rb}}$ and $a_{\mathrm{K,K}}$ are kept constant at their background values [46,50]. Thus, $a_{\mathrm{Rb,K}}$ is a single and well-controlled parameter to obtain a large variety of ground states. To create shell-shaped ground states, there are lower $a^{\mathrm{min}}_{\mathrm{Rb,K}}$ and upper $a^{\mathrm{max}}_{\mathrm{Rb,K}}$ limits for $a_{\mathrm{Rb,K}}$. Indeed, the phase-separation regime only occurs for $g_{12} \geqslant \sqrt{g_{11}g_{22}}$, giving rise to $a^{\mathrm{min}}_{\mathrm{Rb,K}} \approx 72a_0$.[1] However, for $g_{12} \gg \sqrt{g_{11}g_{12}}$, any contact surfaces become energetically unfavorable, resulting in a different type of ground state with side-by-side components [51]. Using the parameters of our reference case and performing three-dimensional simulations [52,53] of the coupled GPEs (1) for increasing $a_{\mathrm{Rb,K}}$, we have located this transition to asymmetric ground states at $a^{\mathrm{max}}_{\mathrm{Rb,K}} \approx 118a_0$. Thus, for $72a_0 \lesssim a_{\mathrm{Rb,K}} \lesssim 118a_0$, a shell-shaped mixture is realized as displayed in Fig. 1, where potassium (orange) forms a shell around rubidium (blue). Moreover, interspecies losses at the core-shell

[1]This lower bound is only approximate. For $a_{\mathrm{Rb,K}} < a^{\mathrm{min}}_{\mathrm{Rb,K}}$ the ground state is shell-shaped but the components increasingly overlap. Nevertheless, the inequality for the phase-separation regime is a good tool to estimate a lower threshold as it depends only on the masses and scattering lengths.

boundary are negligible due to two factors: (i) small overlap between $|\psi_{\mathrm{Rb}}|^2$ and $|\psi_{\mathrm{K}}|^2$, and (ii) the relatively small value of $a_{\mathrm{Rb,K}}$.

III. HOLLOWING TRANSITION AND COLLECTIVE EXCITATION SPECTRUM

Decreasing the scattering length $a_{\mathrm{Rb,K}}$ below $72a_0$ leads to an increasing overlap between the two components. In other words, the repulsion between ^{87}Rb and ^{41}K atoms becomes insufficient for ^{87}Rb to push ^{41}K out of the center of the system, resulting in a nonvanishing particle density of ^{41}K at the center. We call this transition of ^{41}K between a filled and a hollow ground state the *hollowing transition*, in analogy to rf-dressed BECs [19,20]. It is a simple realization of a topological transition, resulting from the appearance of an inner surface in the ^{41}K density.

We expect signatures of the hollowing transition when monitoring the dynamics of the mixture and therefore study its response to perturbations of the ground state. If perturbed in a sufficiently small manner, a BEC reacts linearly and oscillates in the trap with different low-lying collective excitation modes [12,47]. To obtain the corresponding spectrum, we solve the Bogoliubov–de Gennes equations [5,54–56] and perform complementary simulations of the GPEs (1) as discussed in Appendix A.

A key signature of a BEC changing its ground state topology from a filled to a hollow sphere has been identified in the spherically symmetric ($l = 0$) collective excitations of an rf-dressed BEC [19,20]. The corresponding frequencies show a minimum at a certain detuning related to the point of the hollowing transition. The excitation spectrum of a BEC mixture displays a similar feature. Using our reference case, for which the hollowing transition is driven by a change of the intercomponent scattering length $a_{\mathrm{Rb,K}}$, we see a significant fraction of mode frequencies having a minimum at $a_{\mathrm{Rb,K}} \approx 60a_0$, as shown in Fig. 2. This value coincides with the critical value at which the ^{41}K ground state vanishes in the center of the system (vertical dotted line). The excitation spectrum of the mixture helps therefore to identify a key signature of the hollowing transition and a subsequent regime of shell-shaped ground states.

As discussed in Appendix B, a striking difference between an rf-dressed BEC and the mixture is the presence of avoided crossings in the spectrum shown in Fig. 2, which can be traced back to the collective excitations of the inner core component. In our reference case, the disparity of the particle numbers leads to the ground state of ^{87}Rb barely changing when increasing the interaction between the components. Consequently, we see excitation frequencies which are almost independent of $a_{\mathrm{Rb,K}}$ as well as those which tend towards or away from the minimum. At each avoided crossing, the modes exchange the dominant component in the corresponding density oscillations [56] and thus the behavior of their frequency as a function of $a_{\mathrm{Rb,K}}$.

IV. FREE EXPANSION

A special feature of mixture-realized shells is exhibited in their free expansion after the confinement is switched off.

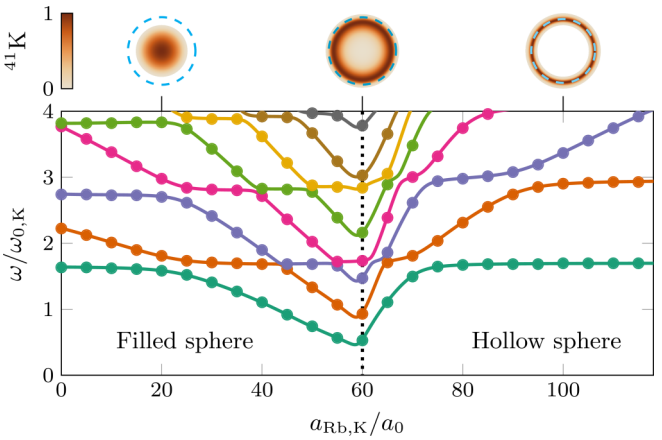

FIG. 2. Mode frequency ω of the lowest-lying spherically symmetric ($l = 0$) collective excitations of the whole system as a function of the interspecies scattering length $a_{\mathrm{Rb,K}}$. The solid lines and dots are determined by the solutions of the Bogoliubov–de Gennes equations and numerical simulations of the GPEs (1), respectively, as discussed in Appendix A. The common minimum of the frequencies is a clear sign of the hollowing transition marked by the dotted vertical line, where $|\psi_{\mathrm{K}}(0)|^2/\max|\psi_{\mathrm{K}}(\mathbf{x})|^2$ drops below 10^{-2}. Top: Two-dimensional cuts of the ground-state density $|\psi_{\mathrm{K}}|^2$ corresponding to the marked values of $a_{\mathrm{Rb,K}}$ (color map scaled to respective peak density) illustrating the hollowing transition. The surface of ^{87}Rb, where $|\psi_{\mathrm{Rb}}|^2$ drops below 10^{-2} of its peak density, is indicated by the dashed blue lines.

Two very distinct expansion scenarios are possible due to the freedom of controlling the intercomponent interaction. Taking a shell-shaped ground state and solely switching off the harmonic confinement for both components leads to an expanding shell as displayed in Fig. 3(a). Here the persisting

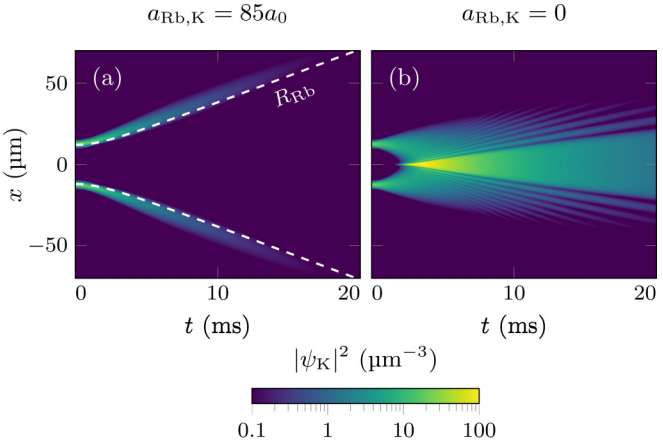

FIG. 3. Time evolution of the spherically symmetric density distribution $|\psi_{\mathrm{K}}|^2$ along the x direction for different free expansion scenarios using the initial shell-shaped state of Fig. 1. (a) Solely switching off the external confinement leads to an expanding shell with its size being proportional to the edge of the expanding inner rubidium core R_{Rb} defined by $|\psi_{\mathrm{Rb}}|^2$ dropping below 10^{-2} of its peak value. (b) By additionally switching off the interaction between the two species at $t = 0$, the shell can expand inwards until it reaches the center and shows a self-interference pattern.

repulsive intercomponent interaction leads to the outwards expansion of the inner component (^{87}Rb), preventing an inwards expansion of the outer component (^{41}K) and therefore the shell structure is conserved. A second scenario occurs, if the inter-component scattering length can be tuned to zero at $t = 0$. In this case, the two components evolve independently and the outer component can expand inwards until it reaches the center and a self-interference pattern emerges, as shown in Fig. 3(b).

Conserving the shell structure during the expansion is an important feature of the mixture compared to rf-dressed shells, where the typical expansion scenario is similar to the one presented in Fig. 3(b) [8,57]. In the case of Fig. 3(a), after $t = 20$ ms, the shell has a radius $\langle r\rangle_{\mathrm{K}} \approx 80$ μm and a width $\sqrt{\langle r^2\rangle_{\mathrm{K}} - \langle r\rangle_{\mathrm{K}}^2} \approx 8$ μm. The natural occurrence of expanding shells presents a clear advantage of our proposed scheme, as they offer the possibility of magnifying dynamical effects like vortex formation and collective excitations on the shell surface.

V. FEASIBILITY OF GENERATING SHELL-SHAPED BECS

Having discussed properties of mixture-based shells in ideal circumstances, we conclude by analyzing the influence of gravity on the mixture. In general, the resulting gravitational sag deforms the shell-creating potential due to the inner species being displaced differently than the outer one. Although small deformations can be compensated by intraspecies repulsion, if the relative displacement becomes too large, the outer species no longer forms a closed shell. Here we want to assess the robustness of the mixture against gravitational sag, which is the most important shell-opening effect for this approach, and point out mitigation strategies.

An ideal shell-shaped BEC is point symmetric with respect to its center. Consequently, we asses the influence of shell-opening effects by comparing the density maxima $n_{\max}(\theta, \varphi)$ and $n_{\max}(\pi - \theta, \varphi + \pi)$ of the ^{41}K ground state $|\psi_K(\mathbf{x})|^2$ along two opposing directions, characterized by the spherical angles θ and φ. Maximizing the difference along all possible directions gives the asymmetry

$$A = \max_{\{\theta,\varphi\}} \left| \frac{n_{\max}(\theta,\varphi) - n_{\max}(\pi-\theta,\varphi+\pi)}{n_{\max}(\theta,\varphi) + n_{\max}(\pi-\theta,\varphi+\pi)} \right|, \qquad (2)$$

which is a measure of how far the shell deviates from the ideal case. A perfect shell yields $A = 0$, whereas the opposite case of a completely opened-up shell gives rise to $A = 1$ because there is at least one direction along which $n_{\max}(\theta, \varphi) = 0$.

We model gravity by including an additional potential $V_{g,\alpha}(z) = m_\alpha g z$ into the single-particle Hamiltonian h_α of each component, where g denotes the gravitational acceleration. As a result, each total single-particle potential retains its harmonic form, but has its minimum shifted by $z_{0,\alpha} = -g/\omega_{0,\alpha}^2$ along the z axis. A nonzero differential shift $\delta z_0 = g|1/\omega_{0,\alpha}^2 - 1/\omega_{0,\beta}^2|$ displaces the two components from each other, thereby deforming the shell. Three solutions offer themselves: (i) realizing equal trap frequencies for both components to achieve equal potential shifts, (ii) working in a microgravity environment to reduce g, or (iii) increasing the trap frequencies, i.e., the laser power. In Earth-based laboratories and following option (i), one could realize shell-shaped BECs by carefully choosing the laser wavelength of the optical trap [58–63]. This is a promising perspective to create quantum bubbles made possible by the method presented in this article. Here, we briefly explore the latter two options and study the degree of microgravity required for closed shells as we vary both the trap frequency and the particle number of the outer species. Figure 4 shows that our reference case indeed requires microgravity conditions to form a closed shell-shaped BEC. On the right-hand side of Fig. 4(a) we mark typical gravitational accelerations provided by available experimental platforms. As indicated by the yellow color, Earth-based laboratories and zero-g planes [64,65] are not suitable, and only for considerably smaller gravitational accelerations, $g \leqslant 10^{-5} g_{\mathrm{E}}$, like on the International Space Station (ISS) [2,66] or in a drop tower [67,68] does the system form an almost ideal shell (dark blue). Depending on the number of particles in the outer species, this threshold varies, potentially allowing an implementation in sounding rockets [69] as well.

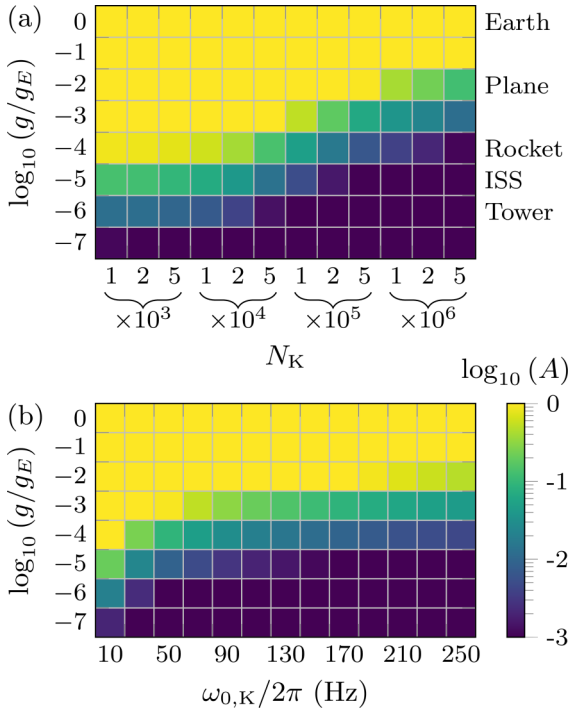

FIG. 4. Asymmetry A, Eq. (2), of a shell-shaped BEC mixture for different gravitational accelerations g ($g_{\mathrm{E}} = 9.81$ m/s^2) and varying (a) numbers of potassium atoms N_{K} or (b) trap frequencies $\omega_{0,\mathrm{K}}$, while keeping the ratio $\omega_{0,\mathrm{K}}/\omega_{0,\mathrm{Rb}} \approx 1.363$. The cases $A = 0$ (dark blue) and $A = 1$ (yellow) correspond to symmetrically filled and opened-up shells, respectively. Existing experimental platforms are marked on the right. The robustness of the shell increases with the particle number due to deformations being compensated by interatomic repulsion within the shell (a) as well as by increasing the trap frequencies at the expense of the overall size of the system (b).

By varying the trap frequencies, Fig. 4(b), we find that going from $\omega_{0,\mathrm{K}} = 2\pi \times 70$ Hz to $\omega_{0,\mathrm{K}} = 2\pi \times 250$ Hz the shell gains robustness against a gravitational acceleration g one order of magnitude larger. This results from a decrease of the absolute gravitational displacement of both components. However, tightening the trap reduces the overall size of the

shell from $\langle r\rangle_{\mathrm{K}} \approx 12.7$ μm down to $\langle r\rangle_{\mathrm{K}} \approx 7.6$ μm in this frequency range. Nevertheless, even weaker trap frequencies ($\omega_{0,\mathrm{K}} = 2\pi \times 10$ Hz) and therefore larger initial shells with a size of $\langle r\rangle_{\mathrm{K}} \approx 27.4$ μm can be achieved under optimal microgravity conditions.

Our study shows that mixtures are excellent tools to create shell-shaped BECs with good spherical symmetry when using drop towers or the International Space Station for which mixture-capable setups such as BECCAL [48] are planned. Depending on the available particle numbers, the trap frequencies may have to be increased to guarantee a good enough symmetry. In future setups special care can be taken about the choice of the laser wavelength and atomic species to achieve equal trap frequencies and allow the generation of shells with perfect symmetry in Earth-based laboratories.

We emphasize that gravity is the *only* major shell-opening effect in the mixture-based scheme. In contrast, the rf-dressed shell BECs do not only require microgravity [26], but are also very sensitive to an inhomogeneity of the rf field and nonperfect alignment with the static magnetic field. Both issues result in a spatially dependent Rabi frequency that tilts the shell-creating potential. Recent modeling of the CAL atom-chip potential reports a tilt equivalent to $10^{-3} g_{\mathrm{E}}$ [3] which would be crippling for the formation of shells made of pure BECs. The big advantage of our proposal is to circumvent this problem entirely while at the same time achieving a similar robustness against gravitational sag alone, as shown in Appendix B.

VI. SUMMARY

We have proposed an alternative method to create spherically symmetric shell-shaped BECs with dual-species atomic mixtures in a microgravity environment. Similar to the conventional rf-dressing scheme, both the ground state and the collective excitations identify the topological transition from a filled sphere to a shell-shaped BEC. Moreover, the shell structure of our mixture is conserved by the repulsive interspecies interaction during free expansion, allowing for a magnification of the dynamics on the shell. Additionally, we have quantified the effects of gravity on the feasibility of achieving symmetrically filled shells and pointed out mitigation strategies.

We emphasize that our scheme based on dual-species mixtures has straightforward applications to related research areas, e.g., few-body physics in mixed dimensions [70,71], ultracold chemistry [72], as well as Bose-Fermi mixtures [73,74] and dipolar BECs [75–77] on curved manifolds.

ACKNOWLEDGMENTS

This project is supported by the German Space Agency (DLR) with funds provided by the Federal Ministry for Economic Affairs and Climate Action (BMWK) due to an enactment of the German Bundestag under Grants No. 50WP1705 (BECCAL), No. 50WM1862 (CAL), and No. 50WM2060 (CARIOQA). A.B. acknowledges funding provided by the Institute of Physics Belgrade, through the grant by the Ministry of Education, Science, and Technological Development of the Republic of Serbia. N.G. acknowledges the support of the German Research Foundation (DFG) within the Project No. A05 of CRC 1227 (DQmat) and under Germany's Excellence Strategy, EXC-2123 QuantumFrontiers, 390837967. The authors are thankful for support by the state of Baden-Württemberg through bwHPC and the German Research Foundation through Grant No. INST 40/575-1 FUGG (JUSTUS 2 cluster).

A.W. and P.B. contributed equally to this work.

APPENDIX A: NUMERICAL SIMULATIONS OF THE GROSS-PITAEVSKII AND BOGOLIUBOV–de GENNES EQUATIONS

To describe collective excitations and to obtain the corresponding spectrum, we use the Bogoliubov–de Gennes equations (BdGEs). Both the GPE (1) and the BdGEs

$$\begin{aligned} E u_\alpha &= L_\alpha u_\alpha + \sum_\beta g_{\alpha\beta}[|\psi_\beta|^2 u_\alpha + |\psi_\alpha||\psi_\beta|(u_\beta + v_\beta)], \\ -E v_\alpha &= L_\alpha^* v_\alpha + \sum_\beta g_{\alpha\beta}[|\psi_\beta|^2 v_\alpha + |\psi_\alpha||\psi_\beta|(u_\beta + v_\beta)] \end{aligned} \tag{A1}$$

for component α of a multicomponent BEC can be derived by extending the calculation presented in Ref. [47]. Here we have suppressed the spatial arguments in the ground state solution $\psi_\alpha(\mathbf{x}) = |\psi_\alpha(\mathbf{x})| e^{iS_\alpha(\mathbf{x})}$ of Eq. (1), the quasiparticle mode functions $u_\alpha(\mathbf{x})$, $v_\alpha(\mathbf{x})$, as well as the linear operator

$$L_\alpha(\mathbf{x}) = -\frac{\hbar^2}{2m_\alpha}[\nabla_{\mathbf{x}} + i\nabla_{\mathbf{x}} S_\alpha(\mathbf{x})]^2 + V_\alpha(\mathbf{x}) - \mu_\alpha. \tag{A2}$$

The chemical potential μ_α is obtained together with the ground state by solving the time-independent GPE numerically. Since the wave functions of the ground states considered throughout this article are real, S_α are constants, $\nabla_{\mathbf{x}} S_\alpha(\mathbf{x}) = 0$, and $L_\alpha^* = L_\alpha$.

The BdGEs (A1) are an eigenvalue problem for the quasiparticle mode functions $\{u_\alpha, v_\alpha\}$ and the corresponding energies $E = \hbar\omega$. The low-frequency modes of the BdGEs describe collective excitations [5], with ω being the frequency of the corresponding density oscillations. In the appendices we suppress mode indices. For more details on the BdGEs we refer to Refs. [5,47].

For our consideration of collective excitations, all potentials and ground states are spherically symmetric. This enables us to perform a separation of variables in the BdGEs by expanding the angular parts in terms of spherical harmonics. The BdGEs thus reduce to a system of linear one-dimensional differential equations with respect to the radial coordinate r, including a centrifugal potential $\hbar^2 l(l+1)/(2m_\alpha r^2)$ with $l = 0, 1, 2, \ldots$. In Fig. 2 (solid lines) we show the first few (positive) mode frequencies ω corresponding to $l = 0$, with the parameters given in Table I and excluding Goldstone modes.

Now we discuss methods for solving Eqs. (1) and (A1). In this article we have performed three different types of numerical simulations: (i) finding the ground state solution of the GPE, (ii) propagating the ground state wave function in time, and (iii) solving the BdGEs. To find the ground states in either one or three dimensions on a discretized grid, we

have used the imaginary-time and split-step methods, giving rise to the results presented in Figs. 1 and 4 [52,53]. A similar simulation but with real time can be used to propagate the ground state wave function in time, which enables us to consider the free expansion scenarios shown in Fig. 3. Additionally, the collective excitation frequencies can be accessed by direct simulation of the GPE (1) and performing a Fourier transformation of a quantity such as the expectation value and variance of the radial coordinate over time. These results are presented by dots in Fig. 2. Finally, for solving the BdGEs we use an eigensolver based on the finite element method.

APPENDIX B: COMPARISON WITH rf-DRESSING APPROACH

In this Appendix we extend our study of the ground state, collective excitation spectrum, free expansion and feasibility to the rf-dressed scheme. We employ the rf-dressed potential [21,23]

$$V_{\mathrm{rf}}(\mathbf{x}) = \frac{M_F g_F}{|g_F|}\sqrt{\left(\frac{m\omega_{0,\mathrm{rf}}^2}{2F}\mathbf{x}^2 - \hbar\Delta\right)^2 + (\hbar\Omega_0)^2}, \qquad \text{(B1)}$$

where M_F denotes the projection of the total momentum F of a dressed state in the hyperfine manifold with corresponding Landé factor g_F. The trap frequency $\omega_{0,\mathrm{rf}}$ of the static magnetic trap is chosen such that the potential of the highest trapped bare state is given by $V_{\mathrm{st}}(\mathbf{x}) = m\omega_{0,\mathrm{rf}}^2\mathbf{x}^2/2$. Moreover, Δ is the detuning of the rf field with respect to the transition between neighboring bare states at the center of the trap, and Ω_0 is the corresponding Rabi frequency. Here we only consider single-component BECs in rf-dressed traps and therefore drop all component-related indices.

1. Ground states

In order to have a fair comparison between the shells created in both systems, we simulate the rf-dressed scheme with the same amount of ^{41}K atoms as in the mixture case. A shell-shaped BEC in the mixture-based approach results from the combination of the harmonic trapping potential and the repulsion provided by the inner ^{87}Rb core, giving rise to an effective potential $V_{\mathrm{eff}}(\mathbf{x}) = g_{\mathrm{Rb,K}}|\psi_{\mathrm{Rb}}(\mathbf{x})|^2 + m_{\mathrm{K}}\omega_{0,\mathrm{K}}^2\mathbf{x}^2/2$ for ^{41}K. To have an rf-dressed shell with the same geometrical parameters, we fit the potential V_{rf}, Eq. (B1), to $V_{\mathrm{eff}}(\mathbf{x})$ and thereby obtain the corresponding values for Δ and $\omega_{0,\mathrm{rf}}$. All other parameters are chosen beforehand and the complete set of parameters is listed in Table II.

Figure 5 presents the ground states of both systems for the parameters given in Table II and clearly shows that the ground-state density distributions of ^{41}K (orange) in the BEC mixture, Fig. 5(b), and the rf-dressed BEC, Fig. 5(d), are almost identical.

2. Collective excitation spectrum

In Fig. 6 we show the collective excitation frequencies for the first few $l = 0$ modes as a function of $a_{\mathrm{Rb,K}}$, (a), or Δ, (b). In the rf-dressed case, this spectrum has a minimum at a certain Δ corresponding to the transition between a filled sphere and a hollow sphere [19,20]. In the mixture case, this spectrum displays a similar feature albeit at a certain value of $a_{\mathrm{Rb,K}}$.

TABLE II. Parameters for the comparison of the two schemes resulting in shells of the same species and with the same geometrical sizes. Note that the parameters for the BEC mixture are the same as in Table I.

	Species	N	$\omega_0/(2\pi)$ (Hz)	$a_{\mathrm{Rb,K}}$ (units of a_0)	$\Delta/(2\pi)$ (kHz)	$\Omega_0/(2\pi)$ (kHz)
rf-dressed BEC	^{41}K[a,b]	10^5	152.3		3.78	2.5
BEC mixture	^{41}K[b]	10^5	70.0	85		
	^{87}Rb[c]	10^6	51.3			

[a]The atoms are prepared in the $|F = 2, M_F = 2\rangle$ dressed state which has a positive Landé factor $g_F = |g_F|$.
[b]$a_{\mathrm{K,K}} = 60a_0$.
[c]$a_{\mathrm{Rb,Rb}} = 100a_0$.

Further similarities can be seen in the limit of the harmonically trapped single-component BEC. In the mixture scheme, this limit corresponds to $a_{\mathrm{Rb,K}} = 0$, where both components are completely decoupled, and are reduced to the well-studied case of a BEC in a spherically symmetric harmonic trap. The collective excitation spectrum

$$\omega_\alpha = \omega_{0,\alpha}\sqrt{2n^2 + 2nl + 3n + l} \qquad \text{(B2)}$$

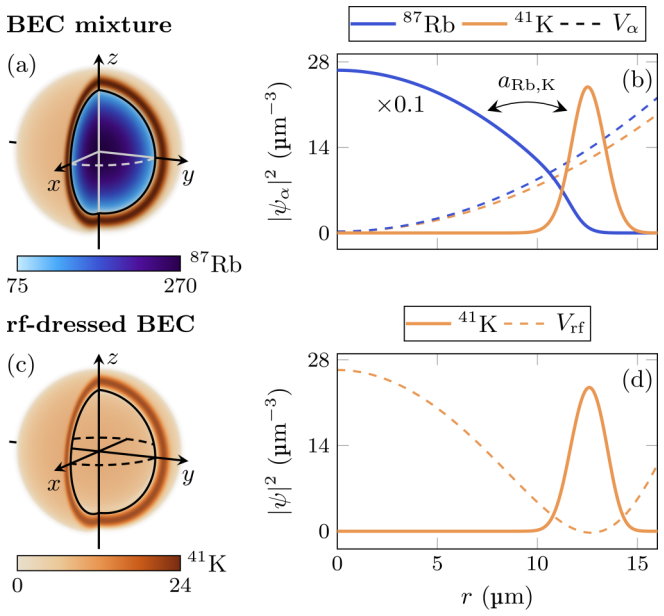

FIG. 5. Spherically-symmetric shell-shaped ground-state density distributions $|\psi_\alpha|^2$ of a ^{87}Rb-^{41}K BEC mixture (a),(b) and an rf-dressed ^{41}K BEC (c),(d) using the parameters presented in Table II. (a),(c) Cut-open three-dimensional density plots (color bar units in μm^{-3}). (b),(d) Density profiles (solid lines) along the radial direction and corresponding trapping potentials (dashed lines) $V_\alpha(\mathbf{x}) = m_\alpha\omega_{0,\alpha}^2\mathbf{x}^2/2$ and $V_{\mathrm{rf}}(\mathbf{x})$, Eq. (B1). The mixture forms a shell due to the interplay between the harmonic confinements and a repulsive interspecies interaction governed by the s-wave scattering length $a_{\mathrm{Rb,K}}$. In contrast, the rf-dressed shell-shaped BEC relies on the trapping potential being a double-well in all directions.

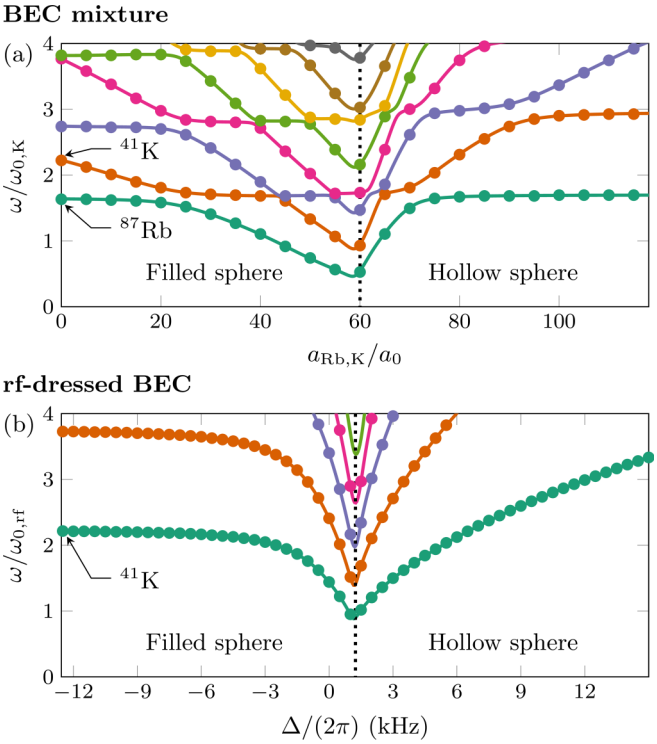

FIG. 6. Mode frequency ω of the lowest-lying $l = 0$ collective excitations for a ^{87}Rb-^{41}K BEC mixture (a) and an rf-dressed ^{41}K BEC (b) as a function of the interspecies scattering length $a_{\mathrm{Rb,K}}$ and detuning Δ, respectively. The solid lines and dots are determined by the solutions of the BdGEs (A1) and numerical simulations of the GPEs (1), accordingly. In both systems the common minimum of the frequencies is a clear sign of the hollowing transition marked by the dotted vertical lines, where $|\psi_{\mathrm{K}}(0)|^2/\max|\psi_{\mathrm{K}}(\mathbf{x})|^2$ drops below 10^{-2}. Moreover, in the respective harmonic limit, where both systems reduce to single-component BECs in spherically symmetric harmonic traps, the excitation frequencies are given by Eq. (B2) and the lowest frequencies are marked accordingly.

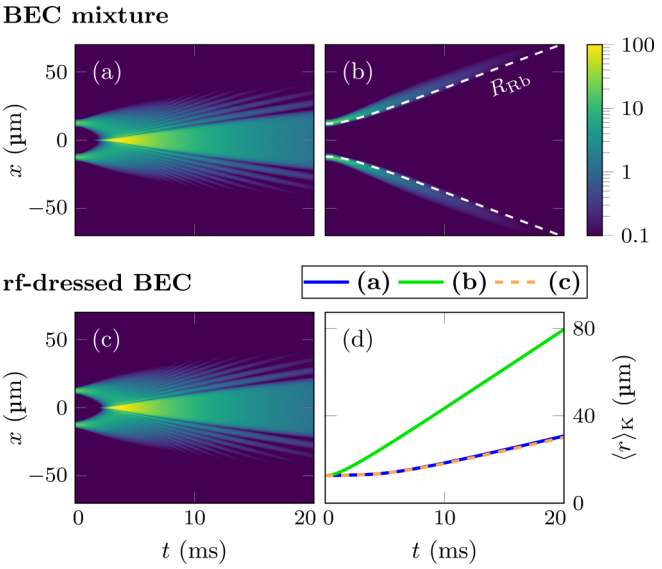

FIG. 7. Free expansion of the spherically symmetric density distributions $|\psi_{\mathrm{K}}|^2$, which are initially prepared in the form presented in Fig. 5, along the x direction for a ^{87}Rb-^{41}K BEC mixture (a),(b) and an rf-dressed ^{41}K BEC (c) (color bar units in $\mu\mathrm{m}^{-3}$). (a) By switching off both the confinement and the interaction between the two species, the shell can expand inwards until it reaches the center and shows a self-interference pattern. (b) Leaving the interaction at $a_{\mathrm{Rb,K}} = 85a_0$ leads to an expanding shell with its size being proportional to the edge of the expanding inner rubidium core R_{Rb} defined by $|\psi_{\mathrm{Rb}}|^2$ dropping below 10^{-2} of its peak value. (c) Switching off all magnetic fields in the rf-dressed BEC results in a similar free expansion as the mixture case in (a). (d) Tracking the expectation value $\langle r\rangle_{\mathrm{K}}$ over time reveals the similarity between (a) and (c) as well as the increasing radius of the expanding shell in (b).

can be obtained analytically using the Thomas-Fermi approximation [47].

Hence, the spectrum depends on the two numbers $n = 0, 1, 2, \ldots$ and $l = 0, 1, 2, \ldots$ as well as the corresponding harmonic trap frequency $\omega_{0,\alpha}$. In Fig. 6(a) we mark the first nonzero excitation frequency for ^{41}K and ^{87}Rb, respectively. At $a_{\mathrm{Rb,K}} = 0$ all shown excitation frequencies agree with Eq. (B2) and can be matched to either of the components.

In the rf-dressed scheme, the harmonic limit corresponds to $\Delta < 0$ with $\Omega_0/|\Delta| \ll 1$, where the potential $V_{\mathrm{rf}}(\mathbf{x})$, Eq. (B1), reduces to a harmonic one with an offset

$$V_{\mathrm{rf}}(\mathbf{x}) \approx -\frac{M_F g_F}{|g_F|}\hbar\Delta + \frac{M_F g_F}{|g_F|}\frac{m\omega_{0,\mathrm{rf}}^2}{2F}\mathbf{x}^2 + O\left(\frac{\Omega_0^2}{\Delta}\right). \quad \text{(B3)}$$

In this limit, the collective excitations of the highest trapped state with $M_F g_F = |g_F|F$ are thus also described by Eq. (B2). Due to the scaling in the respective trap frequency in Fig. 6, the excitation frequencies of the rf-dressed BEC, Fig. 6(b), start at the same value as the excitation frequencies of ^{41}K in the mixture, Fig. 6(a).

Let us now consider the behavior as we move away from the respective harmonic limit by looking at the lowest excitation frequencies, as marked in Fig. 6. In the mixture scheme, increasing the interaction between the components leads to an immediate decrease of the frequencies belonging to ^{41}K. In contrast, the excitation frequencies of ^{87}Rb stay almost constant. This can be explained by the fact that the ground state of ^{87}Rb barely changes while ^{41}K ultimately transforms into a shell which in turn is due to the large disparity between the particle numbers of both components. A consequence of these two different behaviors of the excitation frequencies is the display of avoided crossings. In the rf-dressed scheme, a second component is absent. Furthermore, the behavior of the excitation frequencies is different to those of ^{41}K in the mixture scheme, as they start to decrease only slowly. This is due to the fact that the potential is deformed away from its harmonic form rather slowly and it is only obtaining a double-well-like structure for $\Delta > 0$.

3. Free expansion

In Fig. 7 we compare the free expansions of both ground states displayed in Fig. 5. This is done by switching off the optical dipole trap in the mixture scheme and both the static magnetic and rf field in the rf-dressed scheme. Unsurprisingly, if the interaction between ^{87}Rb and ^{41}K is additionally tuned to zero, $a_{\mathrm{Rb,K}} = 0$, Fig. 7(a), the free expansion of the density distribution $|\psi_{\mathrm{K}}|^2$ is similar to the one reported for

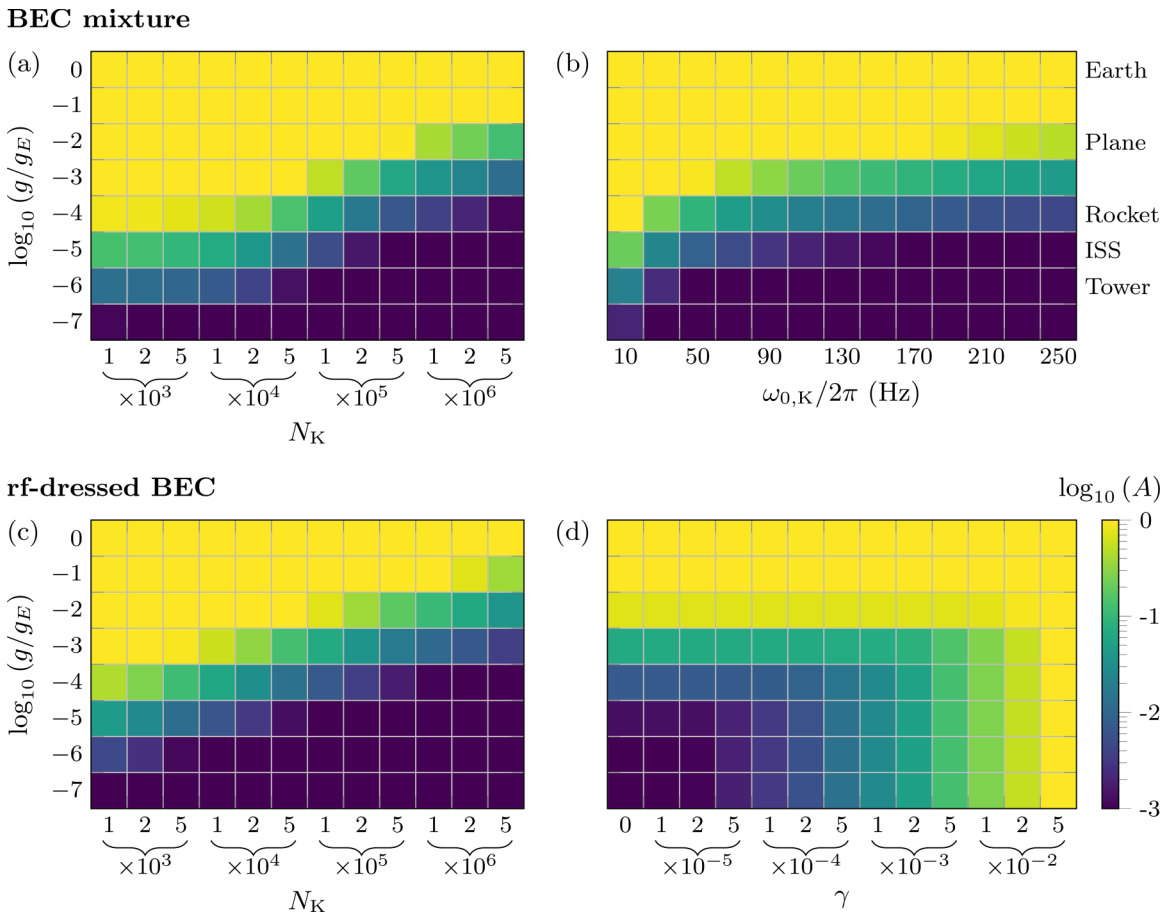

FIG. 8. Asymmetry A, Eq. (2), of a BEC mixture (a), (b) and an rf-dressed BEC (c),(d) for different gravitational accelerations g ($g_E = 9.81$ m/s^2) and varying (a),(c) the numbers of potassium atoms N_K, (b) the trap frequency $\omega_{0,K}$, while keeping the ratio $\omega_{0,K}/\omega_{0,Rb} \approx 1.363$, or (d) the linear gradient γ of the Rabi frequency. The cases $A = 0$ and $A = 1$ correspond to symmetrically filled and opened-up shells, respectively. Existing experimental platforms are marked on the right: Earth-based laboratories, zero-g planes [64,65], sounding rockets [69], the International Space Station [2,66], and a drop tower [67,68]. (a),(c) The robustness of the shell increases with the particle number in a similar fashion for both systems due to deformations being compensated by interatomic repulsion within the shell. (b) Increasing the trap frequencies makes the mixture more robust at the expense of the overall size of the system. (d) The rf-dressed shell opens up both for increasing gravitational acceleration and Rabi frequency inhomogeneity.

the rf-dressed BEC [8,57], Fig. 7(c), due to the fact that both ground states have almost identical shells. In contrast, at $a_{Rb,K} = 85a_0$, Fig. 7(b), the free expansion of $|\psi_K|^2$ is completely different and features an expanding shell. Moreover, for the expansion scenarios shown in Figs. 7(a)–7(c), we track the time-dependent expectation value $\langle r\rangle_K(t) = 4\pi \int_0^\infty dr\, r^3 |\psi_K(\mathbf{x}, t)|^2$ of the radial coordinate for ^{41}K and present the results in Fig. 7(d). Here we see the similarity of the two expansion dynamics displayed in Figs. 7(a) and 7(c) as well as the much faster expanding shell scenario in Fig. 7(b).

4. Feasibility

A comparison of the robustness against shell-opening effects is rather difficult due to the large number of parameters involved. However, a reasonable approach is to compare the robustness against gravity by including a linear potential $V_{g,\alpha}(z) = m_\alpha g z$ in the model of both schemes. Figures 8(a) and 8(c) show the asymmetry A, Eq. (2), of the shells for different levels of gravitational acceleration g and potassium particle numbers N_K. Evidently, without gravity-reducing platforms both systems cannot form closed shells (yellow area). However, in the reference case, $N_K = 10^5$, the rf-dressed BEC is robust against one more order of magnitude of g compared to the mixture. This is due to the difference in the trapping frequencies $\omega_{0,rf}/\omega_{0,K} \approx 2.176$, cf. Table II, as a tighter trap generally increases the robustness. In Fig. 8(b) we vary the trap frequency $\omega_{0,K}$ and achieve a similar robustness as the rf reference case when $\omega_{0,rf} \approx \omega_{0,K} = 2\pi \times 150$ Hz. We emphasize that shell-opening due to gravity can be completely mitigated in the mixture-based scheme when using equal trap frequencies $\omega_{0,K} = \omega_{0,Rb}$, whereas there is no such option in the rf-dressed scheme.

Apart from gravitational sag, rf-dressing has an intrinsic second major shell-opening effect, which is a problem in current realizations. Mainly rooted in inhomogeneities of the rf field, any spatial dependence of the Rabi frequency can open the shell up similar to gravity due to the atoms being forced towards positions of lower frequency where the shell potential is deepest. To study the robustness of the rf-dressed BEC against this effect, we use a simple linear gradient and replace the Rabi frequency Ω_0 in the rf-dressed potential $V_{rf}(\mathbf{x})$, Eq. (B1),

by $\Omega(x) = \Omega_0(1 + \gamma x/x_0)$, where $x_0 = \sqrt{2F\hbar\Delta/(m\omega_{0,\mathrm{rf}}^2)}$ is the position of the minimum of $V_{\mathrm{rf}}(\mathbf{x})$ along the x direction. Hence, at $\mathbf{x} = (\pm x_0, 0, 0)$ the Rabi frequency has a relative deviation of γ compared to its value Ω_0 at $x = 0$, and $\gamma > 0$ tilts the potential towards negative x direction. We chose the Rabi frequency gradient orthogonal to the gravitational acceleration to study the two effects separately. In any other case they may either (partially) compensate or amplify each other.

Figure 8(d) displays how an rf-dressed shell gradually opens up due to either gravity or a gradient in the Rabi frequency. With respect to gravity an experimental platform such as the International Space Station is well suited to create perfectly symmetric shells (dark blue area). However, to achieve this grade of symmetry, the Rabi frequency should not *additionally* deviate more than approximately 10^{-4} between center and surface of the shell. Current modeling of the CAL atom-chip potential reports $\gamma_{\mathrm{exp}} \approx 5 \times 10^{-3}$ for a trap diameter of 71 μm [3,4].

[1] E. R. Elliott, M. C. Krutzik, J. R. Williams, R. J. Thompson, and D. C. Aveline, npj Microgravity **4**, 16 (2018).

[2] D. C. Aveline, J. R. Williams, E. R. Elliott, C. Dutenhoffer, J. R. Kellogg, J. M. Kohel, N. E. Lay, K. Oudrhiri, R. F. Shotwell, N. Yu, and R. J. Thompson, Nature (London) **582**, 193 (2020).

[3] N. Lundblad, R. A. Carollo, C. Lannert, M. J. Gold, X. Jiang, D. Paseltiner, N. Sergay, and D. C. Aveline, npj Microgravity **5**, 30 (2019).

[4] R. A. Carollo, D. C. Aveline, B. Rhyno, S. Vishveshwara, C. Lannert, J. D. Murphree, E. R. Elliott, J. R. Williams, R. J. Thompson, and N. Lundblad, Nature (London) **606**, 281 (2022).

[5] F. Dalfovo, S. Giorgini, L. P. Pitaevskii, and S. Stringari, Rev. Mod. Phys. **71**, 463 (1999).

[6] A. Tononi and L. Salasnich, Phys. Rev. Lett. **123**, 160403 (2019).

[7] N. S. Móller, F. E. A. dos Santos, V. S. Bagnato, and A. Pelster, New J. Phys. **22**, 063059 (2020).

[8] A. Tononi, F. Cinti, and L. Salasnich, Phys. Rev. Lett. **125**, 010402 (2020).

[9] B. Rhyno, N. Lundblad, D. C. Aveline, C. Lannert, and S. Vishveshwara, Phys. Rev. A **104**, 063310 (2021).

[10] N. P. Robins, P. A. Altin, J. E. Debs, and J. D. Close, Phys. Rep. **529**, 265 (2013).

[11] M. Meister, A. Roura, E. M. Rasel, and W. P. Schleich, New J. Phys. **21**, 013039 (2019).

[12] L. P. Pitaevskii and S. Stringari, *Bose-Einstein Condensation and Superfluidity* (Oxford University Press, Oxford, 2016)

[13] A. L. Fetter, Rev. Mod. Phys. **81**, 647 (2009).

[14] A. M. Turner, V. Vitelli, and D. R. Nelson, Rev. Mod. Phys. **82**, 1301 (2010).

[15] K. Padavić, K. Sun, C. Lannert, and S. Vishveshwara, Phys. Rev. A **102**, 043305 (2020).

[16] S. J. Bereta, M. A. Caracanhas, and A. L. Fetter, Phys. Rev. A **103**, 053306 (2021).

[17] J. M. Kosterlitz, Rep. Prog. Phys. **79**, 026001 (2016).

[18] A. Tononi, A. Pelster, and L. Salasnich, Phys. Rev. Research **4**, 013122 (2022).

[19] K. Padavić, K. Sun, C. Lannert, and S. Vishveshwara, Europhys. Lett. **120**, 20004 (2017).

[20] K. Sun, K. Padavić, F. Yang, S. Vishveshwara, and C. Lannert, Phys. Rev. A **98**, 013609 (2018).

[21] O. Zobay and B. M. Garraway, Phys. Rev. Lett. **86**, 1195 (2001).

[22] O. Zobay and B. M. Garraway, Phys. Rev. A **69**, 023605 (2004).

[23] I. Lesanovsky, S. Hofferberth, J. Schmiedmayer, and P. Schmelcher, Phys. Rev. A **74**, 033619 (2006).

[24] B. M. Garraway and H. Perrin, J. Phys. B: At. Mol. Opt. Phys. **49**, 172001 (2016).

[25] H. Perrin and B. M. Garraway, in *Advances in Atomic, Molecular, and Optical Physics*, edited by S. F. Yelin, E. Arimondo, and C. C. Lin (Elsevier Science, Saint Louis, 2017), Vol. 66, pp. 181–262.

[26] Y. Colombe, E. Knyazchyan, O. Morizot, B. Mercier, V. Lorent, and H. Perrin, Europhys. Lett. **67**, 593 (2004).

[27] K. Merloti, R. Dubessy, L. Longchambon, A. Perrin, P.-E. Pottie, V. Lorent, and H. Perrin, New J. Phys. **15**, 033007 (2013).

[28] Y. Guo, R. Dubessy, M. G. de Herve, A. Kumar, T. Badr, A. Perrin, L. Longchambon, and H. Perrin, Phys. Rev. Lett. **124**, 025301 (2020).

[29] Y. Guo, E. M. Gutierrez, D. Rey, T. Badr, A. Perrin, L. Longchambon, V. Bagnato, H. Perrin, and R. Dubessy, arXiv:2105.12981.

[30] T. Schumm, S. Hofferberth, L. M. Andersson, S. Wildermuth, S. Groth, I. Bar-Joseph, J. Schmiedmayer, and P. Krüger, Nat. Phys. **1**, 57 (2005).

[31] I. Lesanovsky, T. Schumm, S. Hofferberth, L. M. Andersson, P. Krüger, and J. Schmiedmayer, Phys. Rev. A **73**, 033619 (2006).

[32] S. Hofferberth, I. Lesanovsky, B. Fischer, J. Verdu, and J. Schmiedmayer, Nat. Phys. **2**, 710 (2006).

[33] S. Hofferberth, B. Fischer, T. Schumm, J. Schmiedmayer, and I. Lesanovsky, Phys. Rev. A **76**, 013401 (2007).

[34] I. Lesanovsky and W. von Klitzing, Phys. Rev. Lett. **99**, 083001 (2007).

[35] W. H. Heathcote, E. Nugent, B. T. Sheard, and C. J. Foot, New J. Phys. **10**, 043012 (2008).

[36] B. E. Sherlock, M. Gildemeister, E. Owen, E. Nugent, and C. J. Foot, Phys. Rev. A **83**, 043408 (2011).

[37] T. L. Harte, E. Bentine, K. Luksch, A. J. Barker, D. Trypogeorgos, B. Yuen, and C. J. Foot, Phys. Rev. A **97**, 013616 (2018).

[38] A. J. Barker, S. Sunami, D. Garrick, A. Beregi, K. Luksch, E. Bentine, and C. J. Foot, New J. Phys. **22**, 103040 (2020).

[39] C. J. Pethick and H. Smith, *Bose–Einstein Condensation in Dilute Gases* (Cambridge University Press, Cambridge, 2008).

[40] W. B. Colson and A. L. Fetter, J. Low. Temp. Phys. **33**, 231 (1978).

[41] T.-L. Ho and V. B. Shenoy, Phys. Rev. Lett. **77**, 3276 (1996).

[42] H. Pu and N. P. Bigelow, Phys. Rev. Lett. **80**, 1130 (1998).

[43] F. Riboli and M. Modugno, Phys. Rev. A **65**, 063614 (2002).

[44] R. Grimm, M. Weidemüller, and Y. B. Ovchinnikov, in *Advances in Atomic, Molecular, and Optical Physics*, edited by B.

Bederson and H. Walther (Academic Press, San Diego, 2000), Vol. 42, pp. 95–170.
[45] E. Timmermans, P. Tommasini, M. Hussein, and A. Kerman, Phys. Rep. **315**, 199 (1999).
[46] C. Chin, R. Grimm, P. Julienne, and E. Tiesinga, Rev. Mod. Phys. **82**, 1225 (2010).
[47] M. Ueda, *Fundamentals and New Frontiers of Bose-Einstein Condensation* (World Scientific, Singapore, 2010).
[48] K. Frye *et al.*, EPJ Quantum Technol. **8**, 1 (2021).
[49] G. Thalhammer, G. Barontini, L. De Sarlo, J. Catani, F. Minardi, and M. Inguscio, Phys. Rev. Lett. **100**, 210402 (2008).
[50] M. Lysebo and L. Veseth, Phys. Rev. A **81**, 032702 (2010).
[51] M. Trippenbach, K. Góral, K. Rzazewski, B. Malomed, and Y. B. Band, J. Phys. B: At. Mol. Opt. Phys. **33**, 4017 (2000).
[52] D. Vudragović, I. Vidanović, A. Balaž, P. Muruganandam, and S. K. Adhikari, Comput. Phys. Commun. **183**, 2021 (2012).
[53] B. Satarić, V. Slavnić, A. Belić, A. Balaž, P. Muruganandam, and S. K. Adhikari, Comput. Phys. Commun. **200**, 411 (2016).
[54] H. Pu and N. P. Bigelow, Phys. Rev. Lett. **80**, 1134 (1998).
[55] D. Gordon and C. M. Savage, Phys. Rev. A **58**, 1440 (1998).
[56] P. Öhberg and S. Stenholm, J. Phys. B: At. Mol. Opt. Phys. **32**, 1959 (1999).
[57] C. Lannert, T.-C. Wei, and S. Vishveshwara, Phys. Rev. A **75**, 013611 (2007).
[58] R. Onofrio and C. Presilla, Phys. Rev. Lett. **89**, 100401 (2002).
[59] R. Onofrio and C. Presilla, J. Stat. Phys. **115**, 57 (2004).
[60] M. S. Safronova, B. Arora, and C. W. Clark, Phys. Rev. A **73**, 022505 (2006).
[61] S. Ospelkaus-Schwarzer, Quantum degenerate fermi-bose mixtures of ^{40}K and ^{87}Rb in 3D optical lattices, Ph.D. thesis, Universität Hamburg, 2006.
[62] J. Ulmanis, S. Häfner, R. Pires, F. Werner, D. S. Petrov, E. D. Kuhnle, and M. Weidemüller, Phys. Rev. A **93**, 022707 (2016).
[63] M. Meister, Novel concepts for ultra-cold quantum gases in microgravity: equal trap frequencies, atoms trapped by atoms, and the space atom laser, Ph.D. thesis, Universität Ulm, 2019.
[64] V. Pletser, S. Rouquette, U. Friedrich, J.-F. Clervoy, T. Gharib, F. Gai, and C. Mora, Microgravity Sci. Technol. **28**, 587 (2016).
[65] B. Barrett, L. Antoni-Micollier, L. Chichet, B. Battelier, T. Lévèque, A. Landragin, and P. Bouyer, Nat. Commun. **7**, 13786 (2016).
[66] N. J. Penley, C. P. Schafer, and J.-D. F. Bartoe, Acta Astronaut. **50**, 691 (2002).
[67] T. van Zoest *et al.*, Science **328**, 1540 (2010).
[68] C. Lotz, Y. Wessarges, J. Hermsdorf, W. Ertmer, and L. Overmeyer, Adv. Space Res. **61**, 1967 (2018).
[69] D. Becker *et al.*, Nature (London) **562**, 391 (2018).
[70] Y. Nishida and S. Tan, Phys. Rev. Lett. **101**, 170401 (2008).
[71] G. Lamporesi, J. Catani, G. Barontini, Y. Nishida, M. Inguscio, and F. Minardi, Phys. Rev. Lett. **104**, 153202 (2010).
[72] J. P. Ríos, *An Introduction to Cold and Ultracold Chemistry* (Springer, Cham, 2020).
[73] K. Mølmer, Phys. Rev. Lett. **80**, 1804 (1998).
[74] C. Ufrecht, M. Meister, A. Roura, and W. P. Schleich, New J. Phys. **19**, 085001 (2017).
[75] S. K. Adhikari, Phys. Rev. A **85**, 053631 (2012).
[76] P. C. Diniz, E. A. B. Oliveira, A. R. P. Lima, and E. A. L. Henn, Sci. Rep. **10**, 4831 (2020).
[77] M. Arazo, R. Mayol, and M. Guilleumas, New J. Phys. **23**, 113040 (2021).